Graphene-Supported Spinel CuFe$_2$O$_4$ Composites: Novel Adsorbents for Arsenic Removal in Aqueous Media

Duong Duc La [1], Tuan Anh Nguyen [2], Lathe A. Jones [1,3] and Sheshanath V. Bhosale [1,*]

[1] School of Science, RMIT University, GPO Box 2476, Melbourne, VIC 3001, Australia; duc.duong.la@gmail.com (D.D.L.); lathe.jones@rmit.edu.au (L.A.J.)
[2] Applied Nanomaterial Laboratory, ANTECH, Hanoi 100000, Vietnam; Tuananhnguyendhb@gmail.com
[3] Centre for Advanced Materials and Industrial Chemistry (CAMIC), School of Science, RMIT University, GPO Box 2476, Melbourne, VIC 3001, Australia
[*] Correspondence: sheshanath.bhosale@rmit.edu.au; Tel.: +61-3-9925-2680; Fax: +61-3-9925-3747

Abstract: A graphene nanoplate-supported spinel CuFe$_2$O$_4$ composite (GNPs/CuFe$_2$O$_4$) was successfully synthesized by using a facile thermal decomposition route. Scanning electron microscopy (SEM), high resolution transmission electron microscopy (HRTEM), Electron Dispersive Spectroscopy (EDS), X-ray diffraction (XRD) and X-ray Photoelectron Spectroscopy (XPS) were employed to characterize the prepared composite. The arsenic adsorption behavior of the GNPs/CuFe$_2$O$_4$ composite was investigated by carrying out batch experiments. Both the Langmuir and Freundlich models were employed to describe the adsorption isotherm, where the sorption kinetics of arsenic adsorption by the composite were found to be pseudo-second order. The selectivity of the adsorbent toward arsenic over common metal ions in water was also demonstrated. Furthermore, the reusability and regeneration of the adsorbent were investigated by an assembled column filter test. The GNPs/CuFe$_2$O$_4$ composite exhibited significant, fast adsorption of arsenic over a wide range of solution pHs with exceptional durability, selectivity, and recyclability, which could make this composite a very promising candidate for effective removal of arsenic from aqueous solution. The highly sensitive adsorption of the material toward arsenic could be potentially employed for arsenic sensing.

Keywords: graphene-supported CuFe$_2$O$_4$ composite; graphene nanoplates; spinel CuFe$_2$O$_4$; arsenic removal; graphene-oxide hybrid material

1. Introduction

Arsenic is highly toxic in the +3 and +5 oxidation state, and is widely present in the environment through leaching from soils, mining activities, fertilizers, industrial wastes, biological activity, and naturally occurring As containing minerals [1,2]. Long-term ingestion and drinking of arsenic contaminated food or water are linked to kidney, skin and lung cancers [3–6]. Therefore, it is of continued importance to remove arsenic from contaminated water, and to provide safe drinking water below the maximum concentration recommended by WHO (<10 ppb). Many approaches have been used for arsenic removal from contaminated water, including adsorption, ion exchange, chemical treatment, reverse osmosis, electrochemical treatment, membrane filtration, and co-precipitation [7–10]. However, due to its simplicity, low cost and high efficiency, adsorption is widely employed and studied as a promising technology for effectively removal of arsenic from contaminated water. The simplicity of these materials is especially important when it is recognized that As contamination is common in the developing world, where treatment processes must be convenient and affordable.

Many adsorbents based on agriculture and industrial waste, surfactants, carbon-base materials, polymers and metal oxides have been employed for arsenic adsorption [11,12]. Among these, metal and metal oxides such as TiO_2 [13–15], nano zero-valent iron [16,17], Fe_2O_3 [3,18,19], Fe_3O_4 [20], CeO_2 [21], CuO [22,23], CaO [24] and ZrO_2 [25,26] have been extensively studied for arsenic treatment in aqueous solution because of their high affinity to arsenic species, low cost, and the tunability of adsorption capacity [12,27]. Recently, considerable attention has been focused on the development of adsorbent composites containing two or more metals as metal oxides, to maximize arsenic adsorption. For instance, Zhang and co-workers synthesized a nanostructured Fe-Cu binary oxide with high adsorption capacity for arsenic [28].

Fe-Mn binary oxides were also successfully fabricated by Shan et al. with a high adsorption capacity toward arsenic [29]. In another report, Yu et al. presented Fe–Ti binary oxide magnetic nanoparticles which combined the photocatalytic oxidation property of TiO_2 with the high adsorption capacity and magnetic properties of γ-Fe_2O_3, for arsenic treatment [30]. Basu et al. found that Fe(III)-Al(III) mixed oxides and Fe(III)-Ce(IV) oxides have a high adsorption capacity toward arsenic [31,32].

Graphene, a two-dimensional (2D) material, has been attracting significant interest in the past decade, due to its exceptional chemical and physical properties which can be applied to many different areas including, but not limited to, electronic devices, energy storage and conversion, sensors, adsorption, and composites [33–38]. Most recently, graphene has gained tremendous interest as a supporting material for enhancement of adsorption properties of adsorbents, due to its large surface area, high conductivity, ionic mobility, and superior mechanical flexibility. For example, Ganesh et al. reported a smart magnetic graphene that removed heavy metals from drinking water [39]. A hybrid of monolithic Fe_2O_3/graphene was also fabricated, and showed favorable properties for arsenic removal [40]. Reduced graphene oxide-supported mesoporous Fe_2O_3/TiO_2 nanoparticles synthesized by a sol-gel route showed high adsorption towards arsenic [41]. Kumar et al. synthesized single-layer graphene oxide with manganese ferrite magnetic nanoparticles for efficient removal of arsenic from contaminated water [42].

In our previous work, we successfully fabricated a graphene nanoplates (GNPs) -supported Fe-Mg binary oxide composite by a simple hydrothermal method. This adsorbent showed a very high adsorption capacity toward arsenic [43]. In continuation of our efforts to this end, herein we report a simple one-pot hydrothermal method to prepare a graphene nanoplates-supported spinel $CuFe_2O_4$ (GNPs/$CuFe_2O_4$) composite. The optimized Cu:Fe molar ratio to fabricate the spinel $CuFe_2O_4$ for arsenic adsorption was adopted from Zhang's work, which is 1:2 [28]. TEM, SEM, EDS, TGA, XPS and XRD were used to characterize the prepared composite. The arsenic adsorption capacity of the material was carefully studied. The effects of parameters including graphene loading, initial arsenic concentration, adsorption time and solution pH on arsenic adsorption, selectivity, and recyclability were investigated through batch experiments and a column test.

2. Materials and Methods

2.1. Materials

Graphene nanoplates (GNPs) were obtained from VNgraphene. Dry acetone, ethanol, sodium hydroxide (NaOH), posstasium hydroxide (KOH), sodium persulfate ($Na_2S_2O_8$), As_2O_5, anhydrous $CuCl_2$ and $FeCl_3$ were purchased from Ajax Finechem. All chemicals were used as received.

2.2. Synthesis of GNPs/$CuFe_2O_4$ Composite

GNPs/$CuFe_2O_4$ composites were fabricated by a simple one-pot hydrothermal strategy. Firstly, $CuCl_2$ and $FeCl_3$ with various Cu:Fe molar ratios of 1:2 were dissolved in 50 mL of ethanol. Then graphene nanoplates with different loadings were dispersed in the mixture solution by sonication for 10 min, and then stirred for 1 h. Subsequently, a 2 M NaOH solution was added dropwise to

the solution under vigorous stirring until a pH of ~8–9 was reached. After 1 h of further stirring, the reaction solution was transferred and sealed in a Teflon-lined autoclave, and placed in an oven pre-heated to 150 °C, for 2 h. Then the solution was cooled to room temperature, and the precipitate was filtered and washed three times each with ethanol and distilled water. The sample was dried overnight at a temperature of 60 °C in air to obtain the $GNPs/CuFe_2O_4$ composites.

2.3. Characterization

The morphology and mapping elemental composition of samples were studied by an EDS-equipped (Oxford Instruments plc, Abingdon, Oxfordshire, UK) scanning electron microscope using an FEI Nova NanoSEM (Hillsboro, AL, USA) operating under high vacuum with an accelerating voltage of 30 keV and an Everhart Thornley Detector (ETD). HRTEM images were obtained on a JEOL 2010 TEM instrument operated at an accelerating voltage of 100 kV. A BrukerAXS D8 Discover instrument with a general area detector diffraction system (GADDS) using a Cu Kα source was utilized to obtain XRD patterns. X-ray photoelectron spectra (XPS) were obtained on a K-Alpha XPS instrument using monochromated aluminum as the X-ray source. The C 1s, Fe 2p, Cu 2p, As 3d and O 1s core level spectra were recorded with an overall resolution of 0.1 eV. The core level spectra were background corrected using the Shirley algorithm, and chemically distinct species were resolved using a nonlinear least square fitting procedure.

2.4. Adsorption Studies

A stock solution of 1000 ppm As(V) was prepared by dissolving As_2O_5 in water. Arsenic concentrations were determined using an Agilent 4200 microwave plasma-atomic emission spectrometer (MP-AES). All samples were analyzed within 24 h of filtration.

2.4.1. Effect of GNPs Loading on Arsenic Sorption

Adsorption experiments were carried out in closed glass vessels. Typically, 24 mg of each adsorbent prepared from different GNP loadings were added into glass vessels containing 50 mL of 10 mg/L arsenic solution at a pH of 4. The solution was kept shaking at 200 rpm at room temperature for 24 h. Then, all samples were filtered by vacuum filtration to remove the adsorbent, and the concentration of arsenic in the residual solutions was analyzed.

2.4.2. Adsorption Isotherm

A total of 10 mg of optimally fabricated adsorbent was added to 50 mL of As(V) solution with initial concentrations ranging from 5 to 90 mg/L in glass vessels. The adsorption was carried out at a solution pH of 4 at room temperature, shaking at a speed of 200 rpm for 24 h. The mixtures were then filtered by vacuum filter and analyzed for residual arsenic by microwave plasma—atomic emission spectrometry (MP-AES).

2.4.3. Adsorption Kinetics

In a typical experiment, 40 mg of $GNPs/CuFe_2O_4$ composite was mixed with 200 mL of 40 mg/L arsenic in a glass vessel. The mixed solution was shaken on an orbital shaker at a speed of 200 rpm at room temperature and solution pH of 4. At certain time intervals, 10 mL of the mixture was taken, filtered by vacuum filter and analyzed for arsenic.

2.4.4. Effect of Solution pH

10 mg of $GNPs/CuFe_2O_4$ composite was added to 50 mL of 10 mg/L arsenic at various solution pH values ranging from 4 to 11 (the pH values were adjusted by dilute HCl and NaOH solutions). The suspensions were shaken at a speed of 200 rpm at room temperature for 24 h. Then, all samples were filtered by vacuum filter and residual arsenic concentrations were determined.

2.4.5. Selectivity Test

10 mg of GNPs/ $CuFe_2O_4$ adsorbent was added to 50 mL of a solution containing 3 mg/L of each ion such as As(V), Na^+, K^+, Ca^{2+} and Mg^{2+}. The mixed solution was shaken on an orbital shaker with a speed of 200 rpm at room temperature and solution pH of 7 for 12 h. The mixtures were then filtered by vacuum filter and analyzed for residual ions by MP-AES.

2.4.6. Recyclability Test

The reusability of the prepared adsorbent was studied by a column test. The GNPs/ $CuFe_2O_4$ oxide composite was assembled as a part of a filter column. Other parts included a glass tube with both ends wrapped with a few layers of filter papers and cotton. The filter column was regenerated by washing several times with 2 M NaOH after each arsenic adsorption cycle before implementing the next experiment.

3. Results and Discussion

The morphology of the obtained graphene nanoplates (GNPs) was studied by SEM (Figure 1). It can be clearly seen in Figure 1a,b that the GNPs had a crumpled, wrinkled morphology with a diameter of tens of microns and a thickness of <20 nm [44].
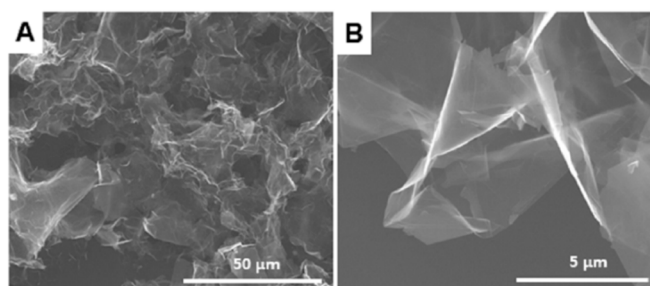

Figure 1. Low (**A**) and high (**B**) scanning electron microscopy (SEM) images of graphene nanoplates.

It is believed that the Fe^{3+} and Cu^{2+} ions firstly physically adsorbed on the GNPs, and then these ions reacted under the hydrothermal conditions to form Fe-Cu binary oxides on the GNPs. The morphology of the as-prepared GNPs/Fe-Cu binary oxides material was investigated by SEM and HRTEM studies. Figure 2a,b and Figure S1 show low and high resolution of SEM images of the composites on a silicon wafer. The SEM images confirmed that the Fe-Cu binary oxides were uniformly dispersed on the surface of the GNPs. The low resolution HRTEM image shown in Figure 2C and Figure S2, also confirmed a good distribution of oxides on the GNPs. When the composite was viewed at the high resolution of HRTEM (Figure 2D), it can be clearly seen that Fe-Cu binary oxides were well-separated, with particle sizes of approximately 5 nm in diameter. The uniform distribution of Fe-Cu binary oxides on the GNPs was further confirmed by EDS mapping (Figure 3). The distribution of Cu and Fe elements on the surface of graphene (elemental C) was uniform and homogeneous.

The EDS study also confirmed that the atomic ratio of Cu:Fe:O is approximately 1:2:4, which was consistent with the theoretical formula of the spinel $CuFe_2O_4$, or a mixture of CuO and Fe_2O_3 oxides formula of obtained binary oxides. In order to further confirm the formation of metal oxides, XRD diffraction patterns were obtained. Figure 4A shows the XRD pattern of the pure $CuFe_2O_4$ and GNPs/Fe-Cu binary oxides composite. In the XRD spectrum of the pure $CuFe_2O_4$, the diffraction peaks at 2θ = 30.56, 36, 43.7, 51.8, 56.6, and 63.1° could be indexed to the (220), (311), (400), (422), (511), and (440) planes of cubic spinel $CuFe_2O_4$ (PDF 06-0545) [45]. When incorporated onto the GNPs surface, the metal oxides mainly formed the cubic spinel structure of $CuFe_2O_4$, as the main diffraction peaks matched with the pure $CuFe_2O_4$. The peaks with asterisks were attributed to the crystallites of the supporting graphene nanoplates [44,46].
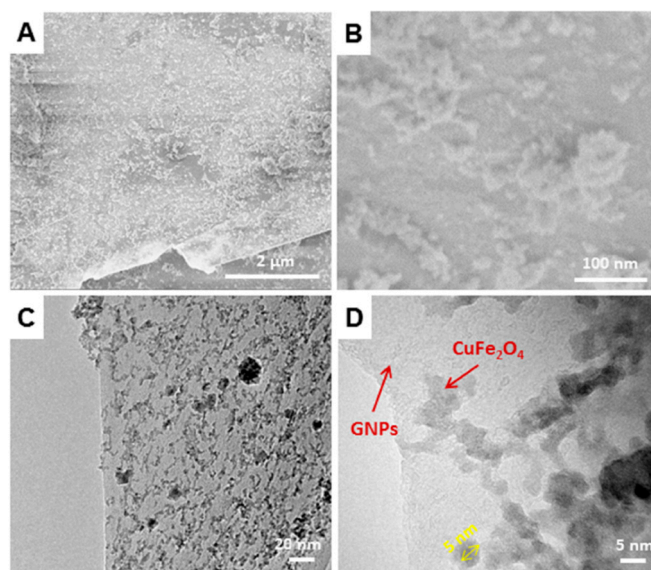
Figure 2. (**A**) and (**B**) SEM images and (**C**) and (**D**) transmission electron microscopy (TEM) images of the GNPs/CuFe$_2$O$_4$ composite.
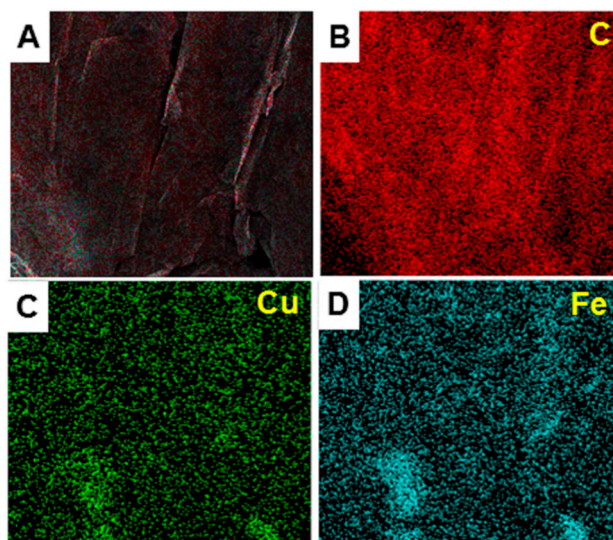

Figure 3. Electron dispersive spectroscopy mappping of the GNPs/CuFe$_2$O$_4$ composite.

The core level XPS spectra of C 1s, Fe 2p and Cu 2p were obtained to probe the chemical environment and oxidation states of C, Fe and Cu in the GNPs/CuFe$_2$O$_4$ composite, as exhibited in Figure 4B–D. The deconvoluted core level of C 1s (Figure 4B) revealed two major peaks at 284.1 and 284.8 eV corresponding to graphenic carbon with C=C (sp2) and C-C (sp3) bonds [47], respectively. In the Figure 4C, the Fe core level XPS spectrum had two dominant peaks at 711.18 and 724.28 eV with small satellite, which was consistent with the Fe 2p3/2 and Fe 2p1/2 of the Fe^{3+} state in the spin-orbit of CuFe$_2$O$_4$, respectively [48]. Figure 4D showed the binding energy of core level Cu 2p. The fitting revealed peaks at around 933.78 and 953.78 eV with a broad satellite at around 942 eV, which corresponded to the Cu2 2p$_{3/2}$ and 2p$_{1/2}$, respectively, of Cu^{2+} in the spinel CuFe$_2$O$_4$ [48]. All of these results further confirmed the formation of CuFe$_2$O$_4$ on the GNPs.

It is of note that the As(V) sorption by the Fe-Cu binary oxide reaches a maximum when the molar ratio of Cu:Fe is 1:2 [28]. Hence, in this study, we have chosen this molar ratio as an optimal condition when preparing the spinel CuFe$_2$O$_4$. We then investigated the effect of graphene loading on

the arsenic sorption capacity by the GNPs/CuFe$_2$O$_4$ composite with an initial As(V) concentration of 24 mg/L, adsorbent dose = 200 mg/L, pH = 4, at room temperature (Figure 5A). It was seen from Figure 5 that the As(V) adsorption was enhanced along with an increase in the GNPs loading, and reached a maximal sorption capacity of about 58 mg/g at the GNPs:CuFe$_2$O$_4$ weight ratio of 1:1 (6:6 in the figure). However, the sorption capacity dramatically dropped as GNPs loading increased above 1:1, and without CuFe$_2$O$_4$, the As(V) sorption capacity by pure GNPs was only 2.38 mg/g. These results demonstrated a significant improvement in As(V) adsorption with the incorporation of GNPs with CuFe$_2$O$_4$.
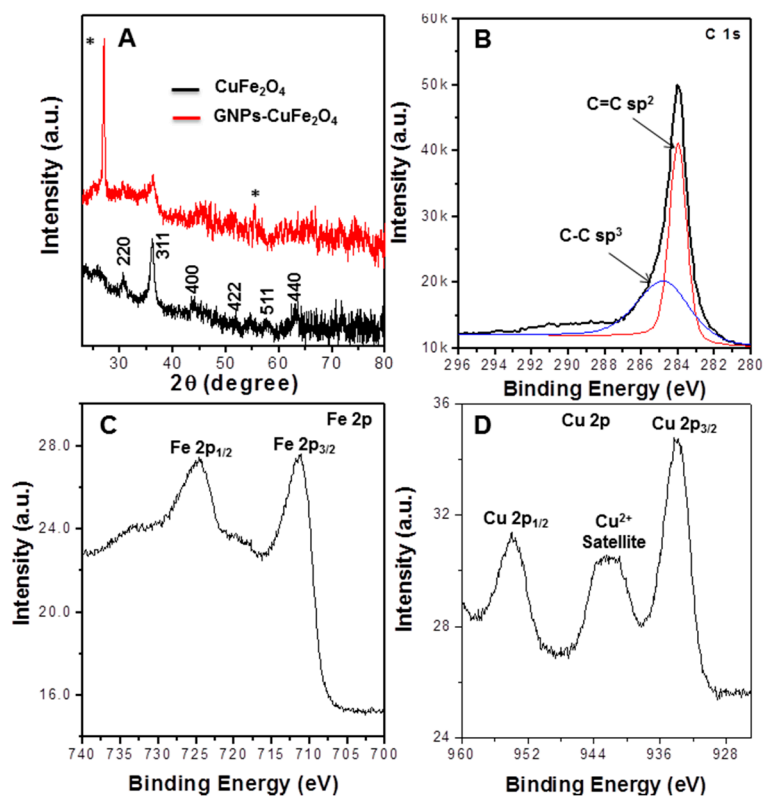
Figure 4. (**A**) X-ray diffraction (XRD) patterns of pure spinel CuFe$_2$O$_4$ and GNPs/CuFe$_2$O$_4$ composites; (**B**–**D**) core level X-ray Photoelectron Spectroscopy pectra of C 1s, Fe 2p and Cu 2p, respectively, obtained from the GNPs/CuFe$_2$O$_4$ composite.

Figure 5B shows the effect of pH on As(V) adsorption by the GNPs/CuFe$_2$O$_4$ composite at an initial As(V) concentration of 10 mg/L, and adsorbent dose = 200 mg/L at room temperature. It is obvious that the sorption capacity of As(V) strongly depended on the solution pH. Arsenic adsorption occurred strongly in acidic conditions with a maximum capacity of 39 mg/g at pH = 4. When the solution pH increased, the adsorption significantly decreased. The change in As(V) adsorption capacity was negligible in the solution pH range of 5 to 9 before declining greatly when the solution pH further increased. This phenomenon may be ascribed to the dependence of adsorption of strong acid anions by metal oxides and hydroxides oxide in solution pH [28]. The pK_a1, pK_a2, pK_a3 of As(V) are 2.1, 6.7, 11.2, which is present in a negative ionic form under most pH conditions. Since the electrostatic attraction is the main force, which is responsible for the adsorption of As(V) on graphene-metal oxide composites [49,50], the change of electrostatic force between As(V) and the GNPs/CuFe$_2$O$_4$ composite may explain the effect of pH on As(V) adsorption. At a low pH, the GNPs/CuFe$_2$O$_4$ adsorbent has a net positive charge due to protonation of –OH groups in the spinel CuFe$_2$O$_4$. As a result, they attract the negatively charged As(V) ions (AsO$_4^{3-}$), which leads to the greater adsorption. When the pH increases, the positive charge decreases, resulting in a decrease of As(V) adsorption.

The leaching of Fe and Cu in the GNPs/CuFe$_2$O$_4$ composite at different pH values was also recorded, as shown in Figure 5B. The release of Fe and Cu was low compared to As(V) adsorption, which indicated that the GNPs/CuFe$_2$O$_4$ composite was a stable and effective adsorbent for arsenic.
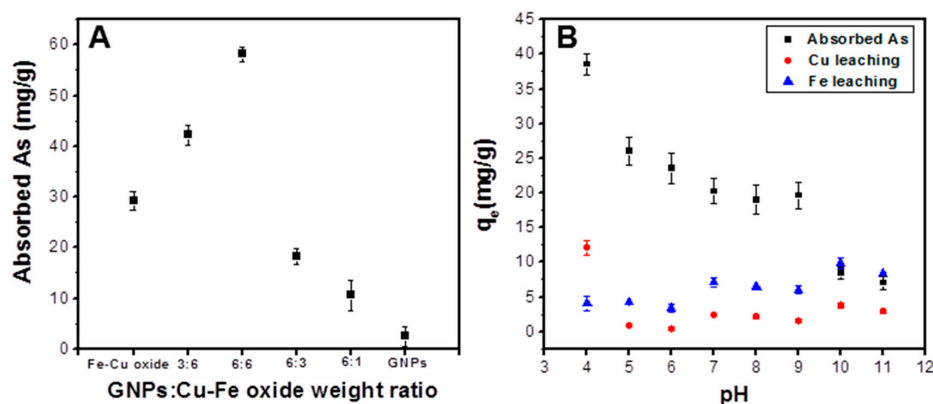
Figure 5. Effect of graphene nanoplates (GNPs) loading (**A**) and solution pH (**B**) on As (V) adsorption by GNPs/CuFe$_2$O$_4$ composites.

The adsorption isotherm was obtained in order to assess the arsenic adsorption and determine the maximum As(V) adsorption capacity by the GNPs/CuFe$_2$O$_4$ composite. The amount of arsenic adsorbed on the composite at equilibrium (q_e) was calculated from different concentrations of arsenic with the following equation:

$$q_e = \frac{(C_0 - C_e) \times V}{m} \tag{1}$$

where C_0 (mg/L) is the initial concentration, C_e (mg/L) is the equilibrium concentration, V (L) is the solution volume, and m (g) is the mass of the GNPs/CuFe$_2$O$_4$ adsorbent.

Figure 6 shows the arsenic adsorption capacity by the composite at equilibrium with various As(V) concentrations in the range of 5–90 mg/L, at an adsorbent dose of 200 mg/L, pH 4 under room temperature. Both adsorption isotherms for the Langmuir and Freundlich models were used to fit the data as expressed in Equations (2) and (3), respectively:

$$q_e = \frac{q_{max} K_L C_e}{1 + K_L C_e} \tag{2}$$

$$q_e = K_F C_e^n \tag{3}$$

where q_e is the amount of arsenic adsorbed on the solid phase at equilibrium (mg/g), q_{max} (mg/g) is the maximum arsenic adsorption capacity per unit weight of adsorbent, C_e is the equilibrium arsenic concentration (mg/L), K_L is the equilibrium adsorption constant represented by the affinity of binding sites (L/mg), K_F is the Freundlich constant, and n is the heterogeneity factor.

The obtained As(V) adsorption constants are presented in Table 1. The higher correlation coefficient (0.966) values of As(V) from the fitted Freundlich plots compared to that of Langmuir plots (0.95) suggested that the Freundlich model was more suitable for representing the adsorption behavior of As(V) by the GNPs/CuFe$_2$O$_4$ composite. The low calculated heterogeneity factor (n = 0.56 for As(V)) also suggests that the Freundlich was the more favorable model. These results indicate that As(V) was heterogeneously adsorbed on the composite surface, suggesting the simultaneous existence of graphene and iron-copper binary oxides in the solid phase. The maximum As(V) adsorption capacity by the GNPs/CuFe$_2$O$_4$ determined from the Langmuir model was 172.27 mg/g, which was a very effective adsorbent for the removal of arsenic. The maximum As(III) adsorption capacity by the GNPs/CuFe$_2$O$_4$ was also determined from the Langmuir model as 236.29 mg/g (Figure S3 and Table S1).
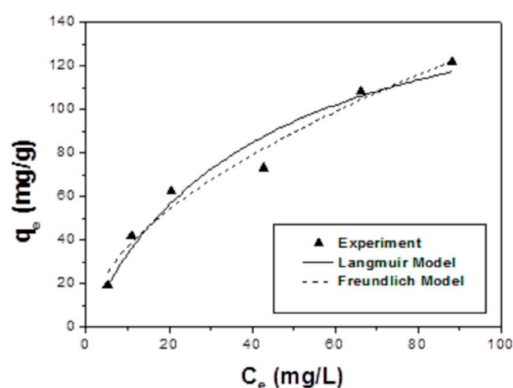
Figure 6. Adsorption isotherm for As(V) by the GNPs/CuFe$_2$O$_4$ composite.

Table 1. Langmuir and Freundlich isotherm parameters for As(V) adsorption on the GNPs/CuFe$_2$O$_4$ composite.

	Langmuir Model			Freundlich Model		
	Q_m (mg/g)	K_L (L/mg)	R^2	K_F	n	R^2
As(V)	172.27	0.02	0.95	10.31	0.56	0.966

Table 2 compares the As(V) adsorption capacity between the GNPs/CuFe$_2$O$_4$ composite with other adsorbents from the literature. It can be seen from the table that the sorption capacity of the GNPs/CuFe$_2$O$_4$ composite was superior to most of the other adsorbents, which could make the GNPs/CuFe$_2$O$_4$ composite a practical adsorbent for arsenic removal.

**Table 2.** Comparison of maximal arsenic adsorption capacity by various adsorbents.

Absorbates	pH	q$_{max}$ (mg/g)	References
Mg$_{0.27}$Fe$_{2.5}$O$_4$	7	83.2	[51]
Fe$_3$O$_4$-GO (MGO)	6.5	59.6	[49]
FeMnO$_x$/RGO	7	22.22	[52]
CeO$_2$-grahene composite	4	1.019	[53]
GO-ZrO(OH)$_2$	5–11	84.89	[50]
nZVI/graphene	7	29	[54]
Magnetic graphene	4	3.26	[39]
Fe$_3$O$_4$/graphene/LDH	6	73.1	[39]
Magnetic-GO	4	38	[55]
Magnetic-rGO	4	12	[55]
MnFe$_2$O$_4$	3	94	[56]
CoFe$_2$O$_4$	3	74	[56]
CuFe$_2$O$_4$ binary oxide	7	82.7	[28]
GNPs/Fe-Mg Oxide	7	103.9	[43]
GNPs/CuFe$_2$O$_4$	4	172.7	This work

In order to further understand the adsorption behavior of As(V) on the GNPs/CuFe$_2$O$_4$ surface, the adsorption kinetics of As(V) adsorption were obtained with an initial As(V) concentration of 40 mg/L (adsorbent dose of 200 mg/L, pH 4 and at room temperature), and sorption capacities were determined at different time intervals (Figure 7). The adsorption quickly reached equilibrium within 2 h. The pseudo-second-order model was applied to describe the kinetic data as expressed in Equation (4):

$$q_t = \frac{Kq_e^2 t}{1 + Kq_e t} \tag{4}$$

where q_t (mg/g) is the amount of arsenic adsorbed on the solid phase at time t (hr), q_e (mg/g) is the amount of arsenic adsorbed on the solid phase at equilibrium, and K is the adsorption rate constant (g mg.h). According to the adsorption kinetic values listed in Table 3, the experimental data was well-fitted, with a correlation coefficient of 0.916. This result implies that the adsorption process may have occurred through chemical adsorption and/or electrostatic attraction, accompanied by electron exchange between the composite and arsenic [57]. The adsorption capacity at equilibrium of the composite with an initial As(V) concentration of 40 mg/L calculated from the pseudo-second-order model was 84.46 mg/g.
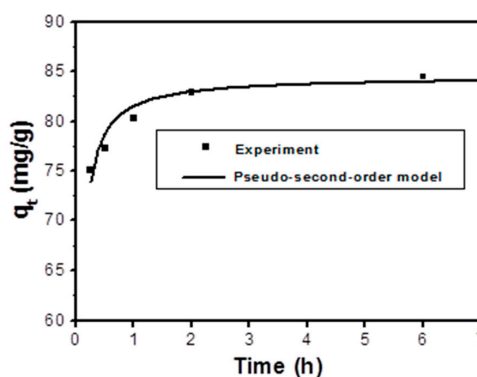

Figure 7. Adsorption kinetics of As(V) on the GNPs/CuFe$_2$O$_4$ composite.

Table 3. Adsorption kinetics parameters for As(V) adsorption on GNPs/CuFe$_2$O$_4$ composite.

Pseudo-Second-Order Model		
q_e (mg/g)	K (h^{-1})	R^2
84.46	0.331	0.916

The XPS As 3d core level spectrum was recorded to verify the presence and chemical state of arsenic on the surface of adsorbent (Figure 8). The appearance of As 3d XPS peak confirmed the presence of arsenic on the surface of the GNPs/CuFe$_2$O$_4$ composite. The core level XPS revealed one dominant peak at 45.5 eV, which was consistent with the binding energy of As(V) [28,58]. As a result, it was obvious that there was no change in oxidation state of As(V) during the sorption process. This further confirmed that arsenic was adsorbed onto the GNPs/CuFe$_2$O$_4$ surface by chemical adsorption and/or an electrostatic attraction mechanism.
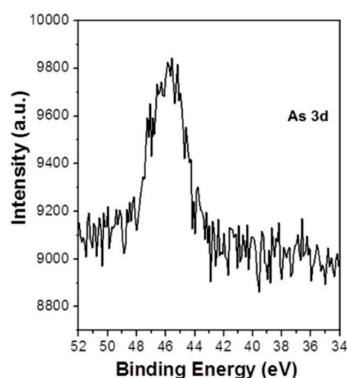

Figure 8. Core level XPS spectra of As 3d obtained from the GNPs/CuFe$_2$O$_4$ composite after adsorption.

Graphene with a large surface area, high conductivity, ionic mobility and superior mechanical flexibility, can be an excellent supporting material for the enhancement of adsorption properties of adsorbents. In this case, $GNPs/CuFe_2O_4$ adsorbent showed enhanced adsorption capacity in comparison with free standing $CuFe_2O_4$ ($q_{max} = 82.7$ mg/g). Based on well-documented understanding and from the discussion above, we proposed a possible adsorption of arsenic by $GNPs/CuFe_2O_4$ (Figure 9). When adding adsorbent into arsenic-containing solution, arsenic is adsorbed on the $CuFe_2O_4$ surface by chemical adsorption and/or electrostatic attraction. The presence of graphene increases the surface area of adsorbent, and as a consequence increases the absorption sites for arsenic.
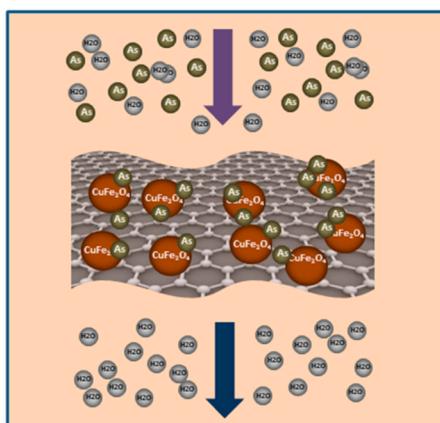
Figure 9. Possible adsorption mechanism of $GNPs/Cu_2FeO_4$ toward arsenic.

Figure 10A shows the selectivity of $GNPs/CuFe_2O_4$ adsorbent towards arsenic in the presence of common positive ions in drinking water such as Na^+, K^+, Ca^{2+} and Mg^{2+}, with an initial concentration of As(V) and other ions at 3 mg/L. It can be seen that while more than 98% of arsenic was adsorbed, there was an insignificant amount of Na^+, K^+ and Ca^{2+} ions adsorbed on the $GNPs/CuFe_2O_4$ composite, indicating that this adsorbent can be effectively and selectively used for arsenic removal. The adsorption capacity of $GNPs/CuFe_2O_4$ composite toward arsenic was also higher than other heavy metals such as lead ions (Figure S4).
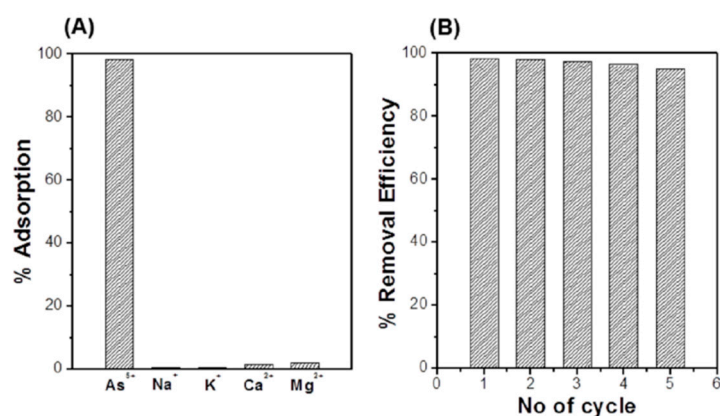
Figure 10. Selectivity (**A**) and recyclability (**B**) of the $GNPs/CuFe_2O_4$ composite for As(V) removal in a column test.

To evaluate recyclability, a filter column with a diameter of 2 cm and a height of 10 cm was assembled, as shown in Figure S5. The mass of the $GNPs/CuFe_2O_4$ composite used was 200 mg. The adsorption process was carried out with 10 mL of flow solution (pH 7) of 3 mg/L As(V). After adsorption, the filter column was washed with 20 mL of 2 M NaOH solution to regenerate the

adsorbent before the next test cycle. The adsorption-regeneration process was repeated for five cycles. The result in Figure 10B shows an insignificant decrease of removal efficiency (less than 4%) after 5 cycles, suggesting that the $GNPs/CuFe_2O_4$ composite has high durability for arsenic removal.

4. Conclusions

A graphene-supported spinel $CuFe_2O_4$ composite was conveniently synthesized by co-precipitating graphene nanoplates with iron and copper ions in ethanol solution. The $CuFe_2O_4$ was crystallized and well-dispersed on the graphene surface. The prepared $GNPs/CuFe_2O$ composite showed fast, high adsorption capacity toward As(V), with a maximum adsorption capacity of 172.27 mg/g at pH 4, which is superior to the majority of reported adsorbents. This adsorbent showed excellent selectivity toward arsenic ions over common metal ions such as Na^+, K^+, Ca^{2+} and Mg^{2+}. The arsenic adsorption by the $GNPs/CuFe_2O$ composite was very effective over a wide range of solution pHs. Moreover, the absorbent could be readily regenerated and recycled for arsenic removal. With these excellent results, it could be concluded that the $GNPs/CuFe_2O$ composite could be considered a promising candidate for practical arsenic removal from aqueous solution. Furthermore, the $GNPs/CuFe_2O$ composite can be potentially used as a sensor probe of arsenic, based on its high sensitive adsorption toward arsenic.

Supplementary Materials: The following are available online at http://www.mdpi.com/1424-8220/17/6/1292/s1, Figure S1: SEM images of the $GNPs/CuFe_2O_4$ composite, Figure S2: TEM images of the $GNPs/CuFe_2O_4$ composite, Figure S3: Adsorption isotherm for As(III) by $GNPs/CuFe_2O_4$ composite, Table S1: Langmuir and Freundlich isotherm parameters for As(III) adsorption on $GNPs/CuFe_2O_4$ composite, Figure S4: Adsorption of 10 mg $GNPs@Fe_2CuO_4$ composite toward 3 mg/L of As^{5+} and Pb^{2+} for 2 hours, Figure S5: Filter column with a diameter of 2 cm and a height of 10 cm for recyclability.

Author Contributions: D.D.L. performed all the experiment and T.A.N. help for XRD and XPS analysis, L.A.J. monitors the analysis, S.V.B. supervises the research project. All co-authors contributed for the manuscript preparation.

Conflicts of Interest: The authors declare no conflict of interest.

References

1. Kitchin, K.T.; Conolly, R. Arsenic-Induced Carcinogenesis-Oxidative Stress as a Possible Mode of Action and Future Research Needs for More Biologically Based Risk Assessment. *Chem. Res. Toxicol.* **2009**, *23*, 327–335. [CrossRef] [PubMed]

2. Erdoğan, H.; Yalçınkaya, Ö.; Türker, A.R. Determination of inorganic arsenic species by hydride generation atomic absorption spectrometry in water samples after preconcentration/separation on nano ZrO_2/B_2O_3 by solid phase extraction. *Desalination* **2011**, *280*, 391–396. [CrossRef]

3. Tuzen, M.; Çıtak, D.; Mendil, D.; Soylak, M. Arsenic speciation in natural water samples by coprecipitation-hydride generation atomic absorption spectrometry combination. *Talanta* **2009**, *78*, 52–56. [CrossRef] [PubMed]

4. Babazadeh, M.; Hosseinzadeh Khanmiri, R.; Abolhasani, J.; Ghorbani-Kalhor, E.; Hassanpour, A. Synthesis and Application of a Novel Functionalized Magnetic Metal-Organic Framework Sorbent for Determination of Heavy Metal Ions in Fish Samples. *Bull. Chem. Soc. Jpn.* **2015**, *88*, 871–879. [CrossRef]

5. Ding, S.-Y.; Dong, M.; Wang, Y.-W.; Chen, Y.-T.; Wang, H.-Z.; Su, C.-Y.; Wang, W. Thioether-based fluorescent covalent organic framework for selective detection and facile removal of mercury(II). *J. Am. Chem. Soc.* **2016**, *138*, 3031–3037. [CrossRef] [PubMed]

6. Akamatsu, M.; Komatsu, H.; Matsuda, A.; Mori, T.; Nakanishi, W.; Sakai, H.; Hill, J.P.; Ariga, K. Visual Detection of Cesium Ions in Domestic Water Supply or Seawater using a Nano-optode. *Bull. Chem. Soc. Jpn.* **2017**, *90*, 678–683. [CrossRef]

7.　Bissen, M.; Frimmel, F.H. Arsenic—A review. Part I: Occurrence, toxicity, speciation, mobility. *Acta Hydroch. Hydrob.* **2003**, *31*, 9–18. [CrossRef]

8.　Mohan, D.; Pittman, C.U. Arsenic removal from water/wastewater using adsorbents—A critical review. *J. Hazard. Mater.* **2007**, *142*, 1–53. [CrossRef] [PubMed]

9.　Jadhav, S.V.; Bringas, E.; Yadav, G.D.; Rathod, V.K.; Ortiz, I.; Marathe, K.V. Arsenic and fluoride contaminated groundwaters: A review of current technologies for contaminants removal. *J. Environ. Manag.* **2015**, *162*, 306–325. [CrossRef] [PubMed]

10.　Singh, R.; Singh, S.; Parihar, P.; Singh, V.P.; Prasad, S.M. Arsenic contamination, consequences and remediation techniques: A review. *Ecotoxicol. Environ. Saf.* **2015**, *112*, 247–270. [CrossRef] [PubMed]

11.　Kurniawan, T.A.; Sillanpää, M.E.; Sillanpää, M. Nanoadsorbents for remediation of aquatic environment: Local and practical solutions for global water pollution problems. *Crit. Rev. Environ. Sci. Technol.* **2012**, *42*, 1233–1295. [CrossRef]

12.　Ray, P.Z.; Shipley, H.J. Inorganic nano-adsorbents for the removal of heavy metals and arsenic: A review. *RSC Adv.* **2015**, *5*, 29885–29907. [CrossRef]

13.　Jézéquel, H.; Chu, K.H. Enhanced adsorption of arsenate on titanium dioxide using Ca and Mg ions. *Environ. Chem. Lett.* **2005**, *3*, 132–135. [CrossRef]

14.　Deedar, N.; Aslam, I. Evaluation of the adsorption potential of titanium dioxide nanoparticles for arsenic removal. *J. Environ. Sci.* **2009**, *21*, 402–408.

15.　Xu, Z.; Li, Q.; Gao, S.; Shang, J.K. As(III) removal by hydrous titanium dioxide prepared from one-step hydrolysis of aqueous TiCl$_4$ solution. *Water Res.* **2010**, *44*, 5713–5721. [CrossRef] [PubMed]

16.　Bhowmick, S.; Chakraborty, S.; Mondal, P.; Van Renterghem, W.; Van den Berghe, S.; Roman-Ross, G.; Chatterjee, D.; Iglesias, M. Montmorillonite-supported nanoscale zero-valent iron for removal of arsenic from aqueous solution: Kinetics and mechanism. *Chem. Eng. J.* **2014**, *243*, 14–23. [CrossRef]

17.　Dong, H.; Guan, X.; Lo, I.M. Fate of As(V)-treated nano zero-valent iron: Determination of arsenic desorption potential under varying environmental conditions by phosphate extraction. *Water Res.* **2012**, *46*, 4071–4080. [CrossRef] [PubMed]

18.　Tang, W.; Li, Q.; Gao, S.; Shang, J.K. Arsenic(III, V) removal from aqueous solution by ultrafine α-Fe$_2$O$_3$ nanoparticles synthesized from solvent thermal method. *J. Hazard. Mater.* **2011**, *192*, 131–138. [CrossRef] [PubMed]

19.　Tang, W.; Li, Q.; Li, C.; Gao, S.; Shang, J.K. Ultrafine α-Fe2O3 nanoparticles grown in confinement of in situ self-formed "cage" and their superior adsorption performance on arsenic(III). *J. Nanopart. Res.* **2011**, *13*, 2641–2651. [CrossRef]

20.　Akin, I.; Arslan, G.; Tor, A.; Ersoz, M.; Cengeloglu, Y. Arsenic (V) removal from underground water by magnetic nanoparticles synthesized from waste red mud. *J. Hazard. Mater.* **2012**, *235*, 62–68. [CrossRef] [PubMed]

21.　Feng, Q.; Zhang, Z.; Ma, Y.; He, X.; Zhao, Y.; Chai, Z. Adsorption and desorption characteristics of arsenic onto ceria nanoparticles. *Nanoscale Res. Lett.* **2012**, *7*, 1–8. [CrossRef] [PubMed]

22.　Reddy, K.; McDonald, K.; King, H. A novel arsenic removal process for water using cupric oxide nanoparticles. *J. Colloid Interface Sci.* **2013**, *397*, 96–102. [CrossRef] [PubMed]

23.　Goswami, A.; Raul, P.; Purkait, M. Arsenic adsorption using copper (II) oxide nanoparticles. *Chem. Eng. Res. Des.* **2012**, *90*, 1387–1396. [CrossRef]

24.　Olyaie, E.; Banejad, H.; Afkhami, A.; Rahmani, A.; Khodaveisi, J. Development of a cost-effective technique to remove the arsenic contamination from aqueous solutions by calcium peroxide nanoparticles. *Sep. Purf. Technol.* **2012**, *95*, 10–15. [CrossRef]

25.　Cui, H.; Su, Y.; Li, Q.; Gao, S.; Shang, J.K. Exceptional arsenic (III, V) removal performance of highly porous, nanostructured ZrO$_2$ spheres for fixed bed reactors and the full-scale system modeling. *Water Res.* **2013**, *47*, 6258–6268. [CrossRef] [PubMed]

26.　Cui, H.; Li, Q.; Gao, S.; Shang, J.K. Strong adsorption of arsenic species by amorphous zirconium oxide nanoparticles. *J. Ind. Eng. Chem.* **2012**, *18*, 1418–1427. [CrossRef]

27.　Habuda-Stanić, M.; Nujić, M. Arsenic removal by nanoparticles: A review. *Environ. Sci. Pollut. Res.* **2015**, *22*, 8094–8123. [CrossRef] [PubMed]

28.　Zhang, G.; Ren, Z.; Zhang, X.; Chen, J. Nanostructured iron (III)-copper (II) binary oxide: A novel adsorbent for enhanced arsenic removal from aqueous solutions. *Water Res.* **2013**, *47*, 4022–4031. [CrossRef] [PubMed]

29. Shan, C.; Tong, M. Efficient removal of trace arsenite through oxidation and adsorption by magnetic nanoparticles modified with Fe-Mn binary oxide. *Water Res.* **2013**, *47*, 3411–3421. [CrossRef] [PubMed]

30. Yu, L.; Peng, X.; Ni, F.; Li, J.; Wang, D.; Luan, Z. Arsenite removal from aqueous solutions by γ-Fe$_2$O$_3$-TiO$_2$ magnetic nanoparticles through simultaneous photocatalytic oxidation and adsorption. *J. Hazard. Mater.* **2013**, *246*, 10–17. [CrossRef] [PubMed]

31. Basu, T.; Ghosh, U.C. Arsenic(III) removal performances in the absence/presence of groundwater occurring ions of agglomerated Fe(III)-Al(III) mixed oxide nanoparticles. *J. Ind. Eng. Chem.* **2011**, *17*, 834–844. [CrossRef]

32. Basu, T.; Ghosh, U.C. Nano-structured iron(III)-cerium(IV) mixed oxide: Synthesis, characterization and arsenic sorption kinetics in the presence of co-existing ions aiming to apply for high arsenic groundwater treatment. *Appl. Surf. Sci.* **2013**, *283*, 471–481. [CrossRef]

33. Novoselov, K.S.; Geim, A.K.; Morozov, S.; Jiang, D.; Zhang, Y.; Dubonos, S.A.; Grigorieva, I.; Firsov, A. Electric field effect in atomically thin carbon films. *Science* **2004**, *306*, 666–669. [CrossRef] [PubMed]

34. Bunch, J.S.; Van Der Zande, A.M.; Verbridge, S.S.; Frank, I.W.; Tanenbaum, D.M.; Parpia, J.M.; Craighead, H.G.; McEuen, P.L. Electromechanical resonators from graphene sheets. *Science* **2007**, *315*, 490–493. [CrossRef] [PubMed]

35. Katsnelson, M.I. Graphene: Carbon in two dimensions. *Mater. Today* **2007**, *10*, 20–27. [CrossRef]

36. Kopelevich, Y.; Esquinazi, P. Graphene physics in graphite. *Adv. Mater.* **2007**, *19*, 4559–4563. [CrossRef]

37. Morozov, S.; Novoselov, K.; Katsnelson, M.; Schedin, F.; Elias, D.; Jaszczak, J.; Geim, A. Giant intrinsic carrier mobilities in graphene and its bilayer. *Phys. Rev. Lett.* **2008**, *100*, 016602. [CrossRef] [PubMed]

38. Becerril, H.A.; Mao, J.; Liu, Z.; Stoltenberg, R.M.; Bao, Z.; Chen, Y. Evaluation of solution-processed reduced graphene oxide films as transparent conductors. *ACS Nano* **2008**, *2*, 463–470. [CrossRef] [PubMed]

39. Gollavelli, G.; Chang, C.-C.; Ling, Y.-C. Facile synthesis of smart magnetic graphene for safe drinking water: heavy metal removal and disinfection control. *ACS Sustain. Chem. Eng.* **2013**, *1*, 462–472. [CrossRef]

40. Ye, J.-H.; Liu, J.; Wang, Z.; Bai, Y.; Zhang, W.; He, W. A new Fe^{3+} fluorescent chemosensor based on aggregation-induced emission. *Tetrahedron Lett.* **2014**, *55*, 3688–3692. [CrossRef]

41. Babu, C.M.; Vinodh, R.; Sundaravel, B.; Abidov, A.; Peng, M.M.; Cha, W.S.; Jang, H.-T. Characterization of reduced graphene oxide supported mesoporous Fe$_2$O$_3$/TiO$_2$ nanoparticles and adsorption of As(III) and As(V) from potable water. *J. Taiwan Inst. Chem. Eng.* **2016**, *62*, 199–208. [CrossRef]

42. Kumar, S.; Nair, R.R.; Pillai, P.B.; Gupta, S.N.; Iyengar, M.; Sood, A. Graphene oxide-MnFe$_2$O$_4$ magnetic nanohybrids for efficient removal of lead and arsenic from water. *ACS Appl. Mater. Interfaces* **2014**, *6*, 17426–17436. [CrossRef] [PubMed]

43. La, D.D.; Patwari, J.M.; Jones, L.A.; Antolasic, F.; Bhosale, S.V. Fabrication of a GNP/Fe-Mg Binary Oxide Composite for Effective Removal of Arsenic from Aqueous Solution. *ACS Omega* **2017**, *2*, 218–226. [CrossRef]

44. La, M.; Duc, D.; Bhargava, S.; Bhosale, S.V. Improved and A Simple Approach For Mass Production of Graphene Nanoplatelets Material. *ChemistrySelect* **2016**, *1*, 949–952. [CrossRef]

45. Zhao, Y.; He, G.; Dai, W.; Chen, H. High catalytic activity in the phenol hydroxylation of magnetically separable CuFe$_2$O$_4$-reduced graphene oxide. *Ind. Eng. Chem. Res.* **2014**, *53*, 12566–12574. [CrossRef]

46. Zhu, J.; Sadu, R.; Wei, S.; Chen, D.H.; Haldolaarachchige, N.; Luo, Z.; Gomes, J.; Young, D.P.; Guo, Z. Magnetic graphene nanoplatelet composites toward arsenic removal. *ECS J. Solid State Sci. Technol.* **2012**, *1*, M1–M5. [CrossRef]

47. Mateo, D.; Esteve-Adell, I.; Albero, J.; Royo, J.F.S.; Primo, A.; Garcia, H. 111 oriented gold nanoplatelets on multilayer graphene as visible light photocatalyst for overall water splitting. *Nat. Commun.* **2016**, *7*, 1–8. [CrossRef] [PubMed]

48. Nedkov, I.; Vandenberghe, R.; Marinova, T.; Thailhades, P.; Merodiiska, T.; Avramova, I. Magnetic structure and collective Jahn-Teller distortions in nanostructured particles of CuFe$_2$O$_4$. *Appl. Surf. Sci.* **2006**, *253*, 2589–2596. [CrossRef]

49. Sheng, G.; Li, Y.; Yang, X.; Ren, X.; Yang, S.; Hu, J.; Wang, X. Efficient removal of arsenate by versatile magnetic graphene oxide composites. *RSC Adv.* **2012**, *2*, 12400–12407. [CrossRef]

50. Luo, X.; Wang, C.; Wang, L.; Deng, F.; Luo, S.; Tu, X.; Au, C. Nanocomposites of graphene oxide-hydrated zirconium oxide for simultaneous removal of As(III) and As(V) from water. *Chem. Eng. J.* **2013**, *220*, 98–106. [CrossRef]

51. Tang, W.; Su, Y.; Li, Q.; Gao, S.; Shang, J.K. Superparamagnetic magnesium ferrite nanoadsorbent for effective arsenic (III, V) removal and easy magnetic separation. *Water Res.* **2013**, *47*, 3624–3634. [CrossRef] [PubMed]

52. Zhu, J.; Lou, Z.; Liu, Y.; Fu, R.; Baig, S.A.; Xu, X. Adsorption behavior and removal mechanism of arsenic on graphene modified by iron–manganese binary oxide (FeMnO x/RGO) from aqueous solutions. *RSC Adv.* **2015**, *5*, 67951–67961. [CrossRef]

53. Yu, L.; Ma, Y.; Ong, C.N.; Xie, J.; Liu, Y. Rapid adsorption removal of arsenate by hydrous cerium oxide–graphene composite. *RSC Adv.* **2015**, *5*, 64983–64990. [CrossRef]

54. Wang, C.; Luo, H.; Zhang, Z.; Wu, Y.; Zhang, J.; Chen, S. Removal of As(III) and As(V) from aqueous solutions using nanoscale zero valent iron-reduced graphite oxide modified composites. *J. Hazard. Mater.* **2014**, *268*, 124–131. [CrossRef] [PubMed]

55. Yoon, Y.; Park, W.K.; Hwang, T.-M.; Yoon, D.H.; Yang, W.S.; Kang, J.-W. Comparative evaluation of magnetite–graphene oxide and magnetite-reduced graphene oxide composite for As(III) and As(V) removal. *J. Hazard. Mater.* **2016**, *304*, 196–204. [CrossRef] [PubMed]

56. Zhang, S.; Niu, H.; Cai, Y.; Zhao, X.; Shi, Y. Arsenite and arsenate adsorption on coprecipitated bimetal oxide magnetic nanomaterials: $MnFe_2O_4$ and $CoFe_2O_4$. *Chem. Eng. J.* **2010**, *158*, 599–607. [CrossRef]

57. Azizian, S. Kinetic models of sorption: A theoretical analysis. *J. Colloid Interface Sci.* **2004**, *276*, 47–52. [CrossRef] [PubMed]

58. Ouvrard, S.; De Donato, P.; Simonnot, M.; Begin, S.; Ghanbaja, J.; Alnot, M.; Duval, Y.; Lhote, F.; Barres, O.; Sardin, M. Natural manganese oxide: Combined analytical approach for solid characterization and arsenic retention. *Geochim. Cosmochim. Acta* **2005**, *69*, 2715–2724. [CrossRef]